CHEMISTRY OF MATERIALS

Article

pubs.acs.org/cm

C–H Bond Activation by Pd-substituted CeO_2: Substituted Ions versus Reduced Species

Lauren M. Misch,[†] Joshua A. Kurzman,[†] Alan R. Derk,[‡] Young-Il Kim,[§] Ram Seshadri,*[,†,⊥] Horia Metiu,[†] Eric W. McFarland,[‡] and Galen D. Stucky[†,⊥]

[†]Department of Chemistry & Biochemistry, [‡]Department of Chemical Engineering, and [⊥]Materials Department and Materials Research Laboratory, University of California, Santa Barbara, California 93106, United States

[§]Department of Chemistry, Yeungnam University, Gyeongsan, Gyeongbuk 712-749, Republic of Korea

Supporting Information

ABSTRACT: Substituted metal oxides containing ionic species have been attracting a great deal of attention because of their potential ability to reduce the usage of precious metals in heterogeneous catalysts. We investigate Pd-substituted CeO_2 for C–H bond activation reactions including the partial oxidation and dry reforming of CH_4. This catalyst has been previously studied for CO oxidation, NO_x reduction, and the water-gas shift reaction. Pd-substituted CeO_2, $Ce_{1-x}Pd_xO_{2-\delta}$, was prepared as a powder with high surface area and a hollow sphere morphology using ultrasonic spray pyrolysis. The catalysts were extensively characterized using synchrotron X-ray diffraction and other techniques, confirming phase pure samples up to 10 mol % Pd substitution. $Ce_{0.95}Pd_{0.05}O_{2-\delta}$ was found to be active for partial oxidation of CH_4 around 500 °C and higher. Our studies, including postcatalytic synchrotron diffraction, suggest that the single-phase $Ce_{1-x}Pd_xO_{2-\delta}$ material is not the active species and that catalysis occurs instead over the reduced two-phase Pd^0/CeO_2. This observation has been further confirmed by verifying the activity of the reduced Pd^0/CeO_2 catalysts for ethylene hydrogenation, a reaction that is known to require Pd^0.

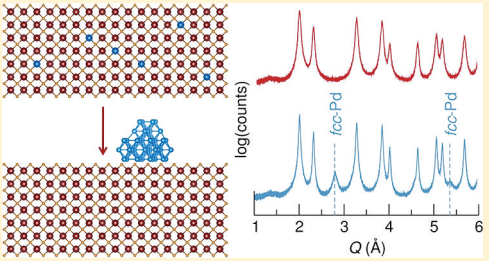

KEYWORDS: *catalyst, nanoparticle, hydrocarbon*

INTRODUCTION

Heterogeneous catalysis on the surfaces of platinum group metals (PGMs) has long been studied, and the fundamental processes are now understood in extraordinary detail from both experimental and theoretical bases. Much less is known about the surface chemistry of PGM species when they exist as ions in solid-state materials such as simple and complex oxides.[1]

In a recent review, Thomas[2] promotes the idea of catalysis on single active sites, well-separated from one another, in a manner that mimics homogeneous catalysis. This important design principle for novel approaches to element-efficient heterogeneous catalysis has been demonstrated through the use of ionic species substituted on cation sites in metal oxides, including the use of Pd^{2+}-substituted metal oxides. Hegde and co-workers[3] have shown conclusively that substituted PGM ions are active for CO removal from gas streams,[4] and as automotive three-way catalysts.[5] Pfefferle and co-workers[6] have found that in CH_4 combustion, the role of PdO and related species is crucial. It has been further suggested that the oxidized state of Pd^{2+} (as opposed to metallic Pd^0) may be the most active species when using substituted complex oxides for catalysis.[7−9] Perhaps the most compelling evidence for using Pd-substituted oxides for heterogeneous catalysis comes from the successful application of "intelligent catalysts" for automotive emissions control.[10]

In this contribution, we use ultrasonic spray pyrolysis (USP) as a simple and clean method to prepare Pd-substituted CeO_2 catalysts with particle sizes in the sub-10 nm range. We have characterized these materials using electron microscopy, X-ray photoelectron spectroscopy, and synchrotron X-ray diffraction (XRD) and observe that Pd substitutes in the lattice at least up to $x = 0.10$ in $Ce_{1-x}Pd_xO_{2-\delta}$.

In this work, $Ce_{1-x}Pd_xO_{2-\delta}$ was tested for C–H bond activation reactions. While there are reports of complete and partial CH_4 oxidation over Pd,[11−15] a wealth of literature has been published on Pd and CeO_2 containing catalysts for CH_4 combustion,[16−23] CO oxidation,[24−27] and NO_x abatement.[28] The oxygen storage capacity of CeO_2 is enhanced when substituted with Pd,[29−33] and doping promotes the formation of oxygen vacancies in catalysis.[5,34,35] It has also been demonstrated that CeO_2 supported catalysts and Pd supported on CeO_2 are active for the water-gas shift reaction.[36−38] Additionally, it was also shown that a Pd-containing catalyst effectively converted CH_4 to a methanol derivative in solution.[39]

The study of CH_4 activation reactions has important energy applications. While large reserves of CH_4 exist and considerable portions of these reserves are currently used to heat homes and generate hydrogen for other synthetic processes, it is widely

Received: September 11, 2011
Revised: November 10, 2011
Published: November 16, 2011

accepted that the conversion of CH_4 to liquid hydrocarbon fuels efficiently with an inexpensive and robust catalyst would be a substantial contribution to alternative energy research.[40] The usual Fischer–Tropsch strategy requires oxidation to mixtures of CO and H_2, which are then converted to higher hydrocarbons. Alternate partial oxidation strategies could be a more direct route to valuable products. For example, dry reforming of CH_4 is of value because recovered CH_4 is often found in the presence of CO_2. As large-scale separations are expensive, it would be convenient to identify a catalyst that efficiently converts CH_4 to useful products in the presence of CO_2.[41]

We address the following questions in this work: (i) Does USP provide a useful route to single-phase Pd-substituted CeO_2 with high surface area? (ii) Can Pd-substituted CeO_2 be used as a catalyst for CH_4 activation in the presence of O_2 (partial oxidation) or CO_2 (dry reforming)? (iii) Can it be concluded that a substituted PGM ion is active for C–H bond activation? We found that Pd-substituted CeO_2 behaves in a manner that is nearly indistinguishable from supported Pd on CeO_2 as a result of the reduction of Pd^{2+} ions to Pd nanoparticles on CeO_2. This study complements prior work on the use of Pt substituted CeO_2 as a catalyst for CH_4 activation.[42]

EXPERIMENTAL SECTION

Pd-substituted CeO_2 was prepared using USP. The USP setup is based on the apparatus described by Skrabalak et al.,[43] which they used for the preparation of nanoporous carbon. The precursor solution, containing $Ce(NO_3)_3{\cdot}6H_2O$ (99%, Aldrich) and $Pd(NO_3)_2{\cdot}2H_2O$ (99.999%, Aldrich) dissolved in the appropriate molar ratios in Millipore water, was nebulized in the custom reaction vessel over a Sunpenton humidifier. The precursor mist was carried by compressed air through a vitreous silica tube in a Lindberg Blue/M tube furnace at 500 °C. Product powders were collected in bubblers containing 4:1 H_2O/EtOH. The suspensions were evaporated in crystallization dishes at 80 °C overnight, and the dry powder was collected.

Room temperature XRD data was collected on a Philips X'PERT diffractometer, and in situ variable temperature diffraction experiments were performed with a Bruker D8 diffractometer equipped with an Anton Parr hot-stage. Synchrotron X-ray powder diffraction patterns were collected in transmission mode at room temperature on beamline 11-BM at the Advanced Photon Source, Argonne National Laboratory, with an X-ray energy of near 30 keV. No evidence for sample degradation or damage was observed. Rietveld refinements were performed using the XND code.[44] X-ray photoelectron spectra were obtained on a Kratos Axis Ultra Spectrometer with a monochromatic Al–Kα source (E = 1486.7 eV). Samples were mounted on a stainless steel sample holder using double-sided carbon tabs. The residual pressure inside the analysis chamber was below 7×10^{-9} Torr. Survey spectra over wide ranges of binding energy were acquired using an analyzer pass energy of 160 eV, and spectra of Pd 3d levels were acquired at a pass energy of 80 eV. Spectra were calibrated to the C 1s peak from adventitious hydrocarbons, expected at a binding energy of 285.0 eV. For peak fitting of the spin–orbit doublets in high resolution scans, the $d_{3/2}$ to $d_{5/2}$ peak area was constrained to a ratio of 2/3.

Scanning electron micrographs (SEMs) were acquired on an FEI XL40 Sirion FEG digital scanning microscope. SEM sample stages were sputtered with Au plasma prior to imaging to reduce sample charging. Transmission electron micrographs (TEMs) were taken on an FEI Tecnai G2 Sphera Microscope. TEM copper-coated Cu grids were prepared by dropcasting a dilute suspension of product in ethanol onto grids. Brunauer–Emmett–Teller (BET) surface area measurements were made on a MicroMetrics TriStar 3000 porosimeter using N_2 as probe gas.

Catalytic testing was carried out in a home-built packed bed reactor, equipped with MKS mass flow controllers and mass spectrometer (SRS) for data acquisition. Quartz tubes (inner-diameter = 4 mm) were packed with 25 mg of catalyst and 50 mg of HPLC grade aluminum oxide (Aldrich) to prevent hotspots, with quartz wool plugs on both ends of the powder. The loosely packed powder occupies a length of 1 cm to maintain a space-time of 0.18 s with a total flow rate of 30 sccm. Reactions were ramped from room temperature to 600 °C at a rate of 10 °C/min. Catalysts were pretreated with Ar, 20% H_2/Ar balance, or 20% O_2/Ar balance. During partial oxidation of CH_4 a 2:1 ratio of CH_4/O_2 was set to flow over the catalyst. This ratio is the stiochiometric amount to produce synthesis gas: $CH_4 + 1/2\ O_2 \rightarrow CO + 2H_2$. All gases had a stated purity of better than 99.99%.

Anticipated products for partial oxidation reactions (2:1 CH_4/O_2) include combustion productions (CO_2 and H_2O), synthesis gas (various ratios of H_2 and CO), oxidative coupling products (C_2H_6, C_2H_4, C_2H_2), and methanol. The mass spectrometer was set to record the activity of the m/z ratios corresponding to these products. While heating any hydrocarbon in the presence of oxygen to high temperatures, combustion products are expected. It is possible for unreacted CH_4 to react with any CO_2 produced from combustion and proceed to do dry reforming of CH_4 to produce synthesis gas (CO + H_2). If CO and H_2 were produced during partial oxidation of CH_4, catalysts were tested for dry reforming of CH_4, in which CH_4 reacts with CO_2 produced from combustion. If CH_4 reacts with CO_2 to produce synthesis gas, then this is a possible mechanistic route for syngas production during partial oxidation reactions.

The anticipated products for dry reforming of CH_4 (1:1 CH_4/CO_2) are synthesis gas (H_2 and CO). The mass spectrometer was set to record the m/z ratios corresponding to all of the products listed for partial oxidation reactions. All subsequent reactions were chosen based on the material's behavior during partial oxidation conditions. Other reactions studied in this work include ethylene hydrogenation (1:1 C_2H_4/H_2) to 300 °C heated at 10 °C/min. Anticipated products of this reaction include ethane and water. The results of characterization of $Ce_{1-x}Pd_xO_{2-\delta}$ and catalytic testing follow.

RESULTS AND DISCUSSION

Characterization of $Ce_{1-x}Pd_xO_{2-\delta}$. Pd-substituted CeO_2 ($Ce_{1-x}Pd_xO_{2-\delta}$) was prepared with x = 0.025, 0.05, 0.075, 0.1 via USP. Representative scanning electron micrographs for a sample with x = 0.05 of the as-prepared powders are shown in Figure 1a. The hollow sphere morphology of the powders is evident in the higher magnification image presented in the inset. The morphology presumably results from evaporation of liquid as the mist traveled through the furnace, leaving behind polydispersed hollow spheres. Despite the relatively large size of the agglomerates, the crystallites of which the spheres are composed are rather fine, with grain sizes on the order of 5 nm, as seen in the transmission electron micrographs of Figure 1b. The $Ce_{0.95}Pd_{0.05}O_{2-\delta}$ powder prepared by USP has BET surface area of about 32 m^2/g.

High-resolution synchrotron X-ray powder diffraction patterns and corresponding Rietveld refinements are shown in Figure 2 for the as-prepared samples and after calcination at 700 °C for 16 h. Pure fluorite CeO_2 is the only phase observed, and no phase segregation occurs in any of the compositions. We did not attempt to prepare materials with Pd concentrations higher than 10 mol %. The diffraction profiles are broader in the substituted materials, relative to pure CeO_2, and this is especially pronounced in the calcined samples (see inset of Supporting Information, Figure S1). Refinements were performed with models fixed at the nominal stoichiometry of each sample ($\delta = x$) with Pd residing on the Ce site, and the atomic displacement parameters (ADP) of Pd and Ce were constrained to the same value. Because the Pd and O occupancies, ADPs, and global scale factor are strongly correlated, the occupancies cannot be refined. For this reason, it is not possible to directly demonstrate the solid solubility of

dx.doi.org/10.1021/cm202709y | Chem. Mater. 2011, 23, 5432–5439

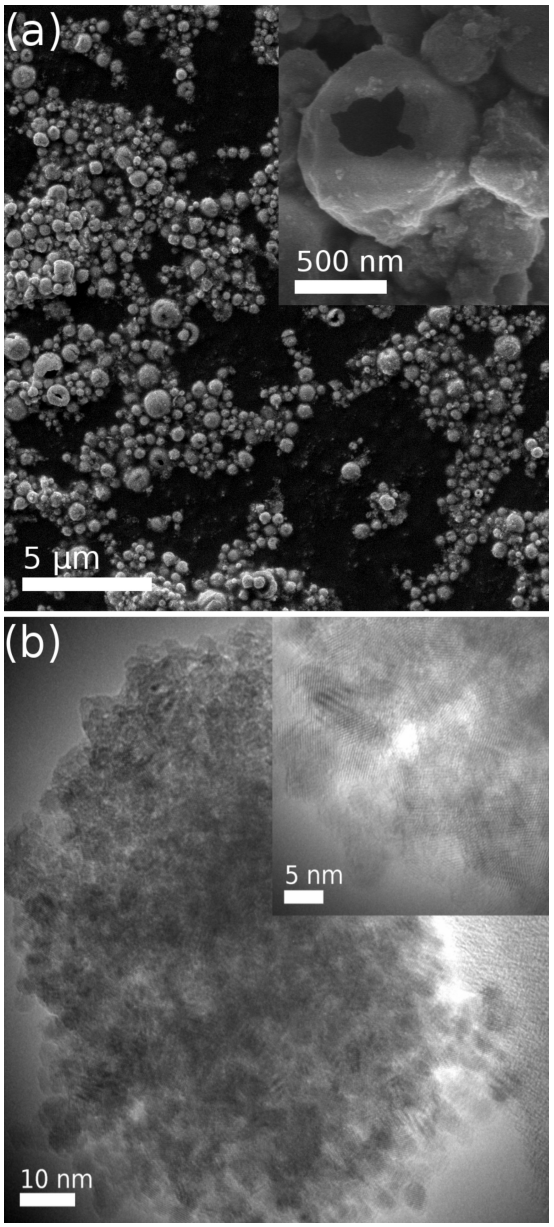

Figure 1. (a) Scanning electron micrograph of $Ce_{0.95}Pd_{0.05}O_{2-\delta}$ particles prepared by nebulized USP showing a hollow sphere morphology. (**b**) Transmission electron micrograph of the $Ce_{0.95}Pd_{0.05}O_{2-\delta}$ particles showing that hollow spheres are composed of approximately 5 nm crystallites, confirming the correlation length obtained from line broadening from synchrotron XRD.

Pd in CeO_2 from average structure (Rietveld) refinement techniques using XRD data.

Thermodiffraction data is presented in the Supporting Information, Figure S1, showing the evolution of the 111 and 200 reflections of CeO_2 between room temperature and 700 °C for unsubstituted CeO_2 ($x = 0$) and 5% Pd-substituted CeO_2 ($x = 0.05$). The thermogravimetric analysis of 5% Pd-substituted CeO_2 ($x = 0.05$) is also shown in the Supporting Information, Figure S2. Diffraction profiles of pure CeO_2 narrow with increasing temperatures, while the peak widths of the substituted material remain significantly broader. The distinct behaviors are indirect evidence that Pd is substituted into the CeO_2 lattice, and suggests that sintering may be suppressed in the substituted material. These points are discussed in greater

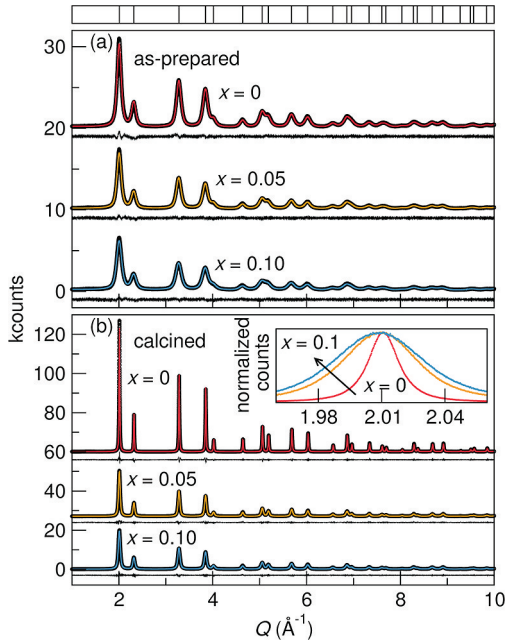

Figure 2. (a) Synchrotron XRD data for as-prepared $Ce_{1-x}Pd_xO_{2-\delta}$ with $x = 0$, 0.05, and 0.1. All samples are single-phase fluorite. Vertical bars in the topmost panel indicate expected fluorite CeO_2 reflection positions. (b) Diffraction from samples after calcining in air for 16 h at 700 °C, with significant peak narrowing because of sintering. The inset shows the strongest reflection, with height normalized, for samples with increasing Pd^{2+} substitution, x. Samples with higher x values are seen to possess significantly broader peaks.

detail with respect to analysis of synchrotron X-ray powder diffraction studies of the $Ce_{1-x}Pd_xO_{2-\delta}$ series.

There are considerable challenges associated with structure determination and refinement of nanoscale materials from Bragg scattering-based diffraction analysis. While it is known that systematic errors arise in the determination of lattice parameters for nanocrystalline materials,[45] this is infrequently acknowledged. Using the Debye function, Palosz and co-workers simulated diffraction patterns for perfect SiC nanocrystallites with sizes ranging from 3 to 8 nm and refined the simulated data by the Rietveld method.[45] Interestingly, they found that in the approximation of a perfect experiment, that is, no sample-offset error, the refined lattice constant was systematically *overestimated*, increasingly as the crystallite size decreased. In refinements approximating an imperfect experiment in which the sample-offset error was allowed to float, the refined lattice constant was increasingly *underestimated* as the crystallite size decreased. Thus, even within the approximation that a nanomaterial is a small single-crystalline piece of the bulk material, Rietveld refinement fails to accurately extract the lattice parameters. In this light, it is clear that great care must be taken when establishing trends in the variation of lattice parameters determined by Rietveld analysis.

The situation is further complicated by the fact that nanocrystallites are not simply small portions of a bulk material. Conventional crystallographic analysis operates on the assumption that the environment of each lattice point is identical. While this may be well approximated by atoms within the core of a nanoparticle, it certainly does not apply to the under-coordinated atoms at or near the surface. For this reason, a single group of lattice constants does not capture the complexity inherent to real nanocrystals. Palosz et al. have

extensively discussed limitations of Rietveld analysis for structure determination in nanocrystalline materials.[45−47]

With these limitations in mind, we address the observed variation of the lattice constant as a function of substitution level with caution. It is clear from the thermodiffraction and synchrotron studies that Pd-substitution in CeO_2 reduces the XRD-coherent correlation length. In Figure 3a, the refined

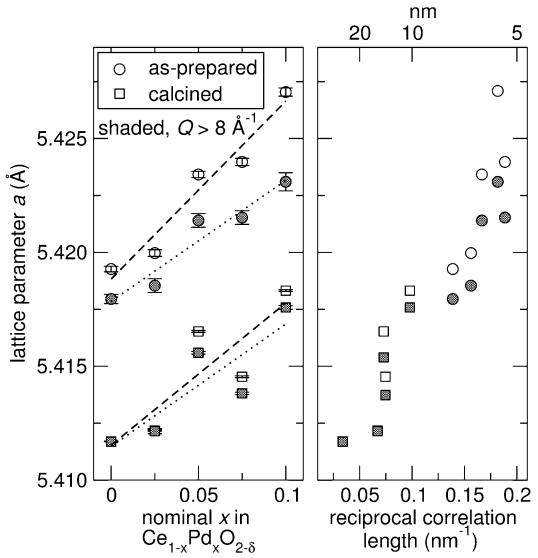

Figure 3. (a) Variation of the cubic cell parameter of $Ce_{1-x}Pd_xO_{2-\delta}$ as a function of nominal Pd substitution x. Data are displayed for as-prepared and calcined samples separately, as described in the text. The cubic cell parameter was determined for the whole Q range of data, and separately for data with $Q > 8$ Å^{-1}, shown with shaded symbols. (b) Cell parameters displayed as a function of the reciprocal crystalline correlation length as obtained from Williamson−Hall analysis of synchrotron XRD data.

lattice parameters of the as-prepared and calcined samples are plotted against the nominal Pd content x. One method for reducing the error associated with lattice parameter determination in nanoparticles is to refine only the high Q portion of a diffraction pattern, although this is only effective in the approximation of a perfect crystallite. Despite this known limitation, the lattice parameters from refining over the entire Q range (open symbols) and only the high Q portion of the patterns (shaded symbols, $Q > 8$ Å^{-1}) are compared in Figure 3a. It is immediately clear that the as-prepared samples appear to have larger lattice constants than the calcined materials. The lattice constants of the as-prepared materials are reduced when only the high Q portions of the patterns are refined; the effect is less pronounced in the calcined materials. $Ce_{1-x}Pd_xO_{2-\delta}$ seems to exhibit Végard style behavior with a lengthening of a as the Pd concentration is increased. This would be consistent with increased cation−cation repulsion arising from the removal of oxygen because of the aliovalent substitution of Pd^{2+} for Ce^{4+}. However, the Shannon−Prewitt ionic radius of 4-coordinate Pd^{2+} (0.64 Å) is significantly smaller than the radius of 8-coordinate Ce^{4+} (0.97 Å), so it is difficult to know whether the observed expansion is an artifact of differences in crystalline correlation lengths, or accurately representative of differences in the lattice constants.

To address whether the variation in the lattice parameter across the series is due to systematic differences in the crystallite sizes, we performed a Williamson−Hall analysis[48] on each of the patterns. It is important to point out that neither Scherrer nor Williamson−Hall analyses are quantitatively accurate methods for extracting correlation lengths, though they do provide reasonable first-order estimates.[45] Additionally, in the case of nanocrystallites of relatively small sizes, < 10 nm, the strain parameter extracted by the WH method carries little physical meaning.[47] We elected to do a Williamson−Hall analysis because it involves fitting over the entire observed Q range, but we note that similar estimates of the correlation lengths were obtained by Scherrer analysis of a single reflection. The refined lattice constants are plotted in Figure 3b as a function of the inverse correlation length estimated from the WH analysis; the volume weighted particle sizes and strains are given in Table 1. As a function of the inverse correlation length,

Table 1. Volume Weighted Particle Sizes (D_v) and Strain (ε) Obtained from a Williamson−Hall Analysis of Synchrotron X-ray Powder Diffraction for $Ce_{1-x}Pd_xO_{2-\delta}$ Where x = 0, 0.025, 0.05, 0.075, 0.1

		calcined			
	as-prepared	(00l)		other reflections	
x	D_v (Å)	D_v (Å)	ε (%)	D_v (Å)	ε (%)
0	72 ± 15	293 ± 2	0.03 ± 1	296 ± 9	0.06 ± 3
0.025	64 ± 11	157 ± 4	0.13 ± 1	149 ± 5	0.16 ± 1
0.05	60 ± 5	118 ± 3	0.11 ± 1	137 ± 1	0.27 ± 1
0.075	53 ± 7	123 ± 5	0.11 ± 2	134 ± 6	0.24 ± 1
0.10	55 ± 12	101	0.16	102 ± 5	0.30 ± 2

the lattice parameters follow an approximately linear trend. It is not possible to conclude whether the observed differences result from systematic errors inherent to the Rietveld method, or whether they genuinely reflect differences between the samples. Within the associated error, the estimated strain is almost constant across the series of as-prepared samples. In the calcined materials, the estimated strain increases significantly in going from the $x = 0$ unsubstituted material to $x = 0.025$, and then gradually increases with the Pd concentration.

It is clear that Rietveld analysis cannot provide direct evidence that Pd substitution occurs in CeO_2, complicated by the many factors we have discussed. Nonetheless, the fact that these are single-phase materials displaying significantly different behavior upon calcination compared to pure CeO_2, coupled with the observation that the XRD-coherent correlation length changes as a function of Pd concentration, are highly suggestive that Pd is dispersed in the CeO_2 lattice. Verification that the nominal Pd concentrations are indeed reflective of the actual compositions is obtained by fully reducing the samples to two-phase mixtures of CeO_2 and *fcc*-Pd metal. A synchrotron XRD pattern and corresponding Rietveld refinement for one such sample (x = 0.05) are shown in Figure 4. The *fcc*-Pd contribution is estimated to be 4.7 mol % by quantitative phase analysis, in excellent agreement with the presumed Pd content.

Scanlon et al. recently described an ab initio study of Pd and Pt substitution in CeO_2 and demonstrated that because of crystal field stabilization effects, the PGM substitutents prefer to displace off the ideal Ce lattice position by about 1.2 Å to adopt square planar coordination, the most common coordination geometry for d^8 cations.[33] This result emphasizes the importance of applying structural probes that are sensitive to local environments. While EXAFS studies have been

dx.doi.org/10.1021/cm202709y | *Chem. Mater.* 2011, 23, 5432−5439

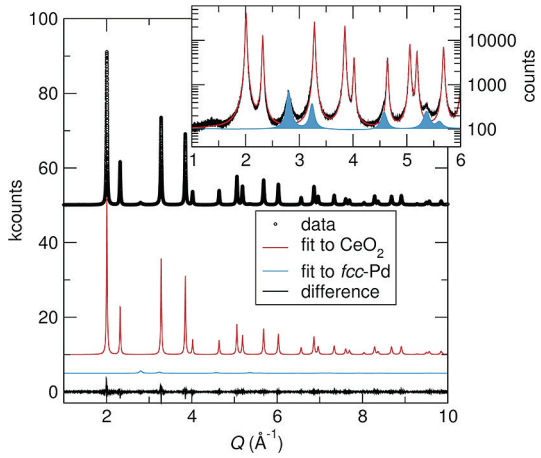

Figure 4. Synchrotron XRD data for $Ce_{0.95}Pd_{0.05}O_{2-\delta}$ reduced in 5% H_2 in Ar at 700 °C for 8 h. The Rietveld refinement shows *fcc*-Pd metal to be quantitatively present with a mole ratio of 0.05.

reported on the $Ce_{1-x}Pd_xO_{2-\delta}$ system,[49,50] we are not aware of any attempts to fit models similar to the one proposed by Scanlon et al.

X-ray photoelectron spectroscopy (XPS) of the Pd 3d region was investigated to determine the charge state of substituted Pd in $Ce_{0.95}Pd_{0.05}O_{2-\delta}$. Indicated in Figure 5 are the binding

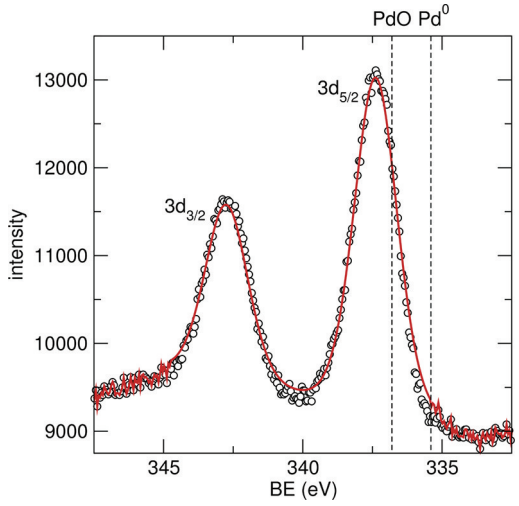

Figure 5. X-ray photoelectron spectrum of the Pd 3d region of as-prepared $Ce_{0.95}Pd_{0.05}O_{2-\delta}$ acquired with a pass energy of 80 eV. The Pd $3d_{5/2}$ peak is shifted to higher binding energy than found in PdO (dashed line indicates position) suggesting a more ionic charge state than that of PdO. No evidence for metallic Pd is seen.

energies for the Pd $3d_{5/2}$ signal in PdO (336.8 eV) and Pd metal (335.4 eV).[51] In Figure 5, the Pd $3d_{5/2}$ signal for $Ce_{0.95}Pd_{0.05}O_{2-\delta}$ is seen at 337.4 eV, a slightly higher binding energy than that of PdO or Pd metal. The increased ionic character suggests Pd lattice substitution. This shift to higher binding energy is in agreement with the XPS of the Pd 3d region taken by Singh et al. for $Ce_{0.95}Pd_{0.05}O_{2-\delta}$ prepared via solution combustion synthesis in which the $3d_{5/2}$ signal is seen at 337.4 eV.[52] Though this does not entirely rule out the possibility of PdO clusters on the surface, both bulk probes like diffraction and surface probes like XPS suggest ionic Pd is incorporated into the CeO_2 lattice. The purpose of this study was also to determine if amorphous PdO, undetectably by XRD, was present on the sample. Because of the low resolution of the XPS data, it would not be possible to deconvolute the two Pd^{2+} signals. However, if amorphous PdO were present, it would crystallize upon calcination.

Reactivity Studies. The $Ce_{1-x}Pd_xO_{2-\delta}$ series was tested for C−H bond activation in partial oxidation of CH_4 and dry reforming of CH_4. Partial oxidation was tested over pure CeO_2 as a control (Figure 6a). Even at 600 °C there is no conversion

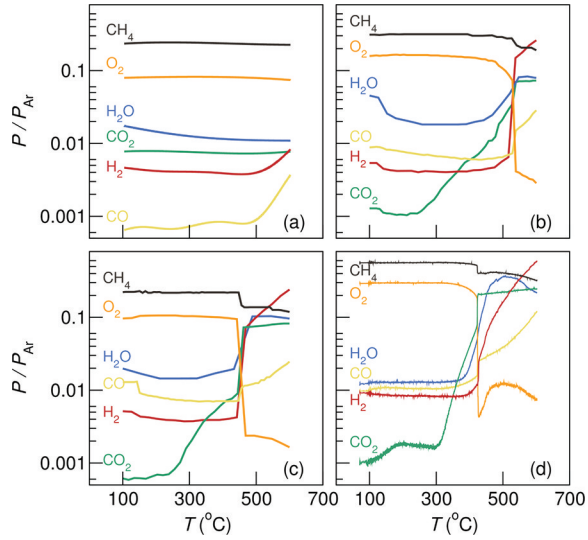

Figure 6. Partial oxidation of methane (2:1 CH_4/O_2) in Ar heated at 10 °C/min to 600 °C over (a) CeO_2, (b) preoxidized (20% O_2 in Ar to 500 °C 1 h) $Ce_{0.95}Pd_{0.05}O_{2-\delta}$, (c) prereduced (20% H_2 in Ar to 500 °C 1 h) $Ce_{0.95}Pd_{0.05}O_{2-\delta}$, and (d) prereduced (20% H_2 in Ar to 500 °C 1 h) PdO/CeO_2. Almost no reaction is observed over pure CeO_2. The substituted Pd catalyst produces combustion products and non-stoichiometric synthesis gas during partial oxidation and behaves similarly to the supported Pd catalyst under reaction conditions.

of CH_4 to products of interest. Whereas the USP prepared CeO_2 was inactive, Figure 6 shows the Pd-substituted CeO_2 catalyst is active for CH_4 combustion.

It was of interest to use a minimum amount of PGM while still achieving C−H bond activation. The quantitative work was performed primarily on $Ce_{0.95}Pd_{0.05}O_{2-\delta}$ which was found by us to be slightly more active than $Ce_{0.975}Pd_{0.025}O_{2-\delta}$ and approximately the same as $Ce_{0.925}Pd_{0.075}O_{2-\delta}$. For partial oxidation of CH_4, $Ce_{0.95}Pd_{0.05}O_{2-\delta}$ was subjected to either prereduction or preoxidation. In both pretreatment cases, the same reaction character is observed. The only difference the pretreatment yields is a slightly lower activation temperature for the prereduced sample. In partial oxidation over $Ce_{0.95}Pd_{0.05}O_{2-\delta}$ (Figures 6b,c), combustion products (CO_2 and H_2O) were observed along with nonstoichiometric synthesis gas. Excess H_2 is produced from the partial oxidation of CH_4 over $Ce_{0.95}Pd_{0.05}O_{2-\delta}$.

To consider if CH_4 is reacting with CO_2 produced from combustion, dry reforming of CH_4 was tested separately. The same two pretreatments were performed individually. The pretreatment makes very little difference in the reaction character and the activation temperature of the catalyst. Very minimal synthesis gas was producing during dry reforming of CH_4 over $Ce_{0.95}Pd_{0.05}O_{2-\delta}$. Dry reforming is not the sole mechanism by which excess H_2 is produced.

dx.doi.org/10.1021/cm202709y | *Chem. Mater.* 2011, 23, 5432–5439

To further probe the mechanism by which partial oxidation of CH_4 over $Ce_{0.95}Pd_{0.05}O_{2-\delta}$ produces excess H_2 a steady state reaction was performed. While the gas ratios for partial oxidation remained the same, the temperature ramp was changed to allow the catalyst to come to steady state at each temperature stage before continuing. The temperature ramping for the steady state reaction was 1 h dwells in 50 °C increments starting at 400 °C, increasing to 600 °C, and back down again. As shown in Figure 7, the steady state reaction clearly shows

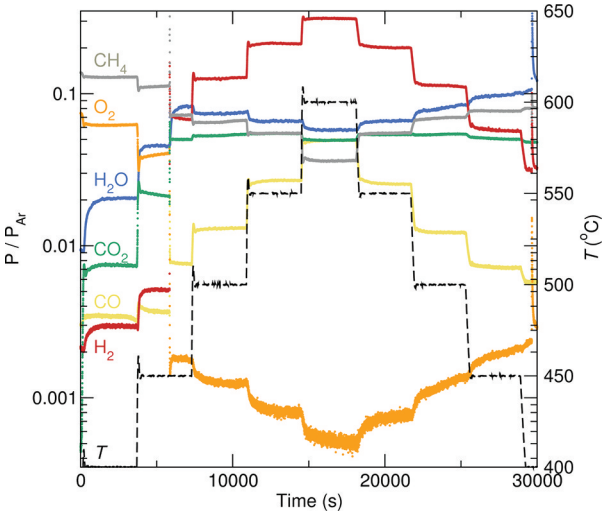

Figure 7. Steady state partial oxidation of methane (2:1 CH_4/O_2) in Ar heated in 50 °C increments from 450 to 600 °C with a dwell time of 1 h at each temperature step over $Ce_{0.95}Pd_{0.05}O_{2-\delta}$. At 450 °C sufficient Pd metal is present to produce nonstoichiometric synthesis gas, H_2 in excess. After combustion, several secondary reactions occur including steam reforming and water gas shift.

consumption of water during partial oxidation of CH_4, suggesting steam reforming. Along with the consumption of water, more CO_2 is produced than expected. This is likely a result of the water-gas shift reaction. The excess H_2 observed during partial oxidation of CH_4 over $Ce_{0.95}Pd_{0.05}O_{2-\delta}$ also likely results from a combination of some dry reforming, steam reforming, and water gas shift reactions. The long time steady state reaction for partial oxidation of methane over $Ce_{0.95}Pd_{0.05}O_{2-\delta}$ was carried out for 24 h at 600 °C (Supporting Information, Figure S3).

To explain why prereduction causes this catalyst to become active at a slightly lower temperature than the preoxidized sample, we chose to further investigate how reducing conditions affected this material. Synchrotron powder XRD of the prereduced catalyst in Figure 4 distinctly shows *fcc*-Pd in addition to cubic CeO_2. It appears that Pd-substituted CeO_2 becomes Pd supported on CeO_2 under reducing conditions, and this is the catalytically active phase for C−H bond activation. Pd-substituted CeO_2 is not active for C−H bond activation. To confirm that the substituted material behaves like Pd metal under reaction conditions, partial oxidation was recorded for a prereduced sample of PdO supported on CeO_2 (Figure 6d). Partial oxidation of CH_4 over Pd metal supported on CeO_2 shows identical reaction character to partial oxidation over the Pd-substituted CeO_2, but with activity for excess hydrogen production igniting at about 400 °C as opposed to about 450 °C in Pd-substituted CeO_2.

The reaction character observed for partial oxidation and dry reforming of methane over Pd-substituted CeO_2 is in contrast to that Pt-substituted CeO_2. Partial oxidation of methane over Pt-substituted CeO_2 does produce stoichiometric synthesis gas between 450 and 500 °C, while Pd-substituted CeO_2 produces nonstoichiometric synthesis gas in the form of excess H_2. Pt-substituted CeO_2 is also active for dry reforming of methane to synthesis gas with relatively high conversion, while Pd-sub ceria produces nonstoichiometric synthesis gas with a very low yield. Pd-substituted CeO_2 likely undergoes several secondary reactions during partial oxidation of methane, including dry reforming of methane, water-gas shift, and steam reforming of methane

The synchrotron powder diffraction pattern was collected for postreaction $Ce_{0.95}Pd_{0.05}O_{2-\delta}$ mixed with Al_2O_3. Just as *fcc*-Pd was seen in the reduced material (Figure 4), so too is this phase observed in the diffraction pattern shown in Figure 8 along with

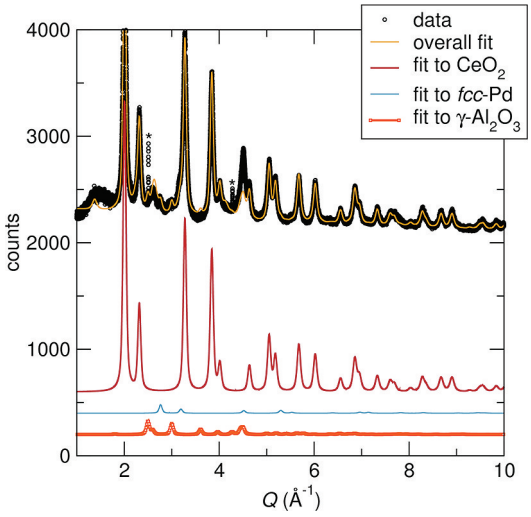

Figure 8. Synchrotron XRD data for $Ce_{0.95}Pd_{0.05}O_{2-\delta}$ mixed with γ-Al_2O_3 after use as catalyst under partial oxidation conditions to 600 °C. The Rietveld refinement shows *fcc*-Pd metal present along with diluent Al_2O_3. The asterisks indicate an unidentified impurity.

the γ-Al_2O_3 diluent. We took special care to cool the material in an inert atmosphere after becoming active under reaction conditions. The material was also handled carefully, quickly contained, and promptly sent for characterization. We recognize that some reoxidation may take place but the *fcc*-Pd phase is very clearly seen in the postreaction material. Certainly no PdO phase is observed in the postreaction material. Moreover, the fact that the catalytic behavior matches that of Pd/CeO_2 further supports that the postreaction material does contain Pd metal. The correlation length of *fcc*-Pd determined from synchrotron XRD and the Scherrer line broadening equation is near 7 nm for postreaction $Ce_{0.95}Pd_{0.05}O_{2-\delta}$ and near 100 nm for the as-prepared Pd/CeO_2 used for comparison. However, it should be noted that the Scherrer line broadening equation does not provide the most accurate measure of coorelation length at these length scales. It seems that the catalytically active phase of $Ce_{0.95}Pd_{0.05}O_{2-\delta}$ for partial oxidation of CH_4 is actually the reduced Pd supported on CeO_2. Other reactions and chemical probes were considered to determine the presence of metallic Pd in this catalyst.

dx.doi.org/10.1021/cm202709y | *Chem. Mater.* 2011, 23, 5432–5439

It would appear that Pd-substituted CeO_2 becomes Pd supported on CeO_2 under reaction conditions. Since Pd supported on oxides is capable of catalyzing ethylene hydrogenation, we performed ethylene hydrogenation over $Ce_{0.95}Pd_{0.05}O_{2-\delta}$.[53] As seen in Figure 9a, no ethane was

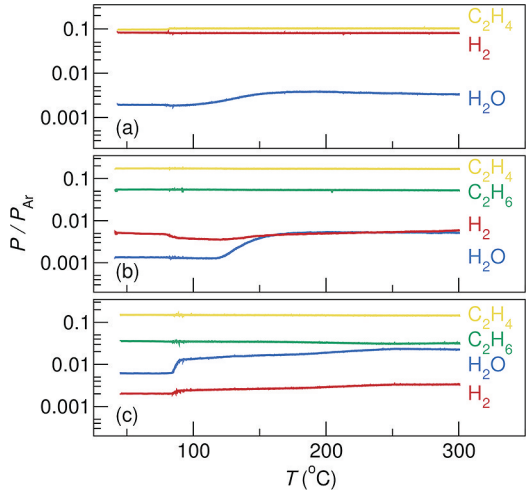

Figure 9. Ethylene hydrogenation (1:1 C_2H_4/H_2) in Ar heated at 10 °C/min to 300 °C over (a) CeO_2, (b) prereduced (20% H_2 in Ar to 300 °C 1 h) $Ce_{0.95}Pd_{0.05}O_{2-\delta}$, (c) prereduced (20% H_2 in Ar to 300 °C 1 h) PdO/CeO_2. The reduced Pd substituted catalyst is active for a reaction known to take place on Pd metal and performs similarly to the supported Pd catalyst.

produced over unsubstituted CeO_2. However, ethane was produced over prereduced $Ce_{0.95}Pd_{0.05}O_{2-\delta}$ at room temperature (Figure 9b). Increasing the temperature did not increase the ethylene conversion in this reaction. The same behavior was observed for reduced PdO/CeO_2 (Figure 9c). It is interesting to note that there appears to be a slightly higher selectivity toward ethane production for reduced $Ce_{0.95}Pd_{0.05}O_{2-\delta}$ than the reduced PdO/CeO_2 used for comparison. To confirm that this reaction proceeds over Pd metal supported on CeO_2, and not the as-prepared $Ce_{0.95}Pd_{0.05}O_{2-\delta}$, we attempted ethylene hydrogenation without a prereduction. The catalyst does not become active until it becomes sufficiently reduced by the ethylene and hydrogen flowing over the catalyst. Figure 10 shows that at around 110 °C the catalyst was reduced to Pd metal supported on CeO_2 at which point ethylene was converted to ethane. The catalyst continued to actively produce ethane while it was cooled back to room temperature.

CONCLUSIONS

Pd-substituted CeO_2 catalysts have been successfully prepared via USP with a surface area of 32 m^2/g and hollow sphere morphology. These materials are phase pure up to 10 mol % Pd substitution. This material becomes catalytically active for C−H bond activation only after the Pt^{2+} ions have been reduced to Pd metal supported on CeO_2. Partial oxidation of CH_4 over $Ce_{0.95}Pd_{0.05}O_{2-\delta}$ yields the expected combustion products along with nonstiochiometric synthesis gas in the form of excess hydrogen gas. The excess hydrogen is a result of several secondary reactions occurring after combustion, including dry reforming of CH_4, steam reforming of CH_4, and water gas shift. The catalytically active phase for this material is Pd supported on CeO_2, confirmed by the ethylene hydrogenation reaction. Additionally, we have identified USP as an adequate method for

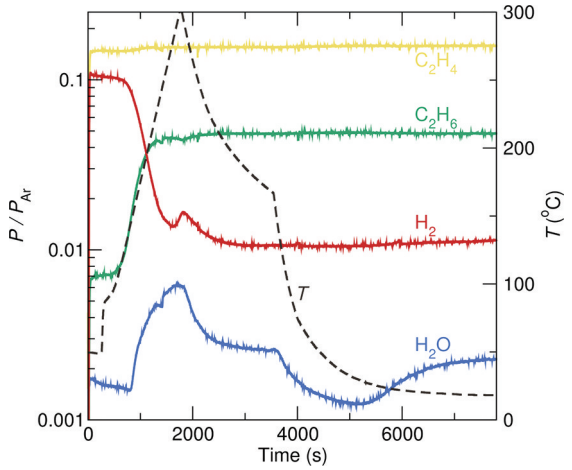

Figure 10. Ethylene hydrogenation (1:1 C_2H_4/H_2) over as-prepared $Ce_{0.95}Pd_{0.05}O_{2-\delta}$ heated at 10 °C/min to 300 °C. The material becomes active and produces C_2H_6 only once the material become sufficiently reduced around 120 °C, further confirming that the catalytically active form of this material is Pd supported on CeO_2.

the preparation of substituted metal oxides and potentially for the preparation of well-dispersed metal nanoparticles on oxide supports upon reduction.

ASSOCIATED CONTENT

Supporting Information

Further details are given in Figures S1−S3. This material is available free of charge via the Internet at http://pubs.acs.org.

AUTHOR INFORMATION

Corresponding Author

*E-mail: seshadri@mrl.ucsb.edu.

ACKNOWLEDGMENTS

This work was supported by the Department of Energy, Office of Basic Energy Sciences through Grant DE-FG02-89ER14048 and Grant DE-FG02-10ER16081. L.M.M. thanks Janet Kayfetz for suggestions on the manuscript. G.D.S. acknowledges support from the University of California Discovery Grant Program GCP08-128649. Use of the Advanced Photon Source was supported by the U.S. Department of Energy, Office of Science, Office of Basic Energy Sciences, under Contract No. DE-AC02-06CH11357. L.M.M. is supported by a Fellowship from the ConvEne IGERT Program (NSF-DGE 0801627). A.R.D. acknowledges the NSF for a Graduate Research Fellowship under Grant DGE 0707430. The use of the shared facilities of the UCSB Materials Research Laboratory: an NSF MRSEC (DMR-1121053), a member of the NSF-funded Materials Research Facilities Network (www.mrfn.org) is gratefully acknowledged.

REFERENCES

(1) Crabtree, R. H. *The organometallic chemistry of the transition metals*; John Wiley & Sons Inc: New York, 2009; p 505.
(2) Thomas, J. M. *J. Chem. Phys.* **2008**, *128*, 182502.
(3) Hegde, M. S.; Madras, G.; Patil, K. C. *Acc. Chem. Res.* **2009**, *42*, 704−712.
(4) Bera, P.; Priolkar, K. R.; Gayen, A.; Sarode, P. R.; Hegde, M. S.; Emura, S.; Kumashiro, R.; Jayaram, V.; Subbanna, G. N. *Chem. Mater.* **2003**, *15*, 2049−2060.

(5) Baidya, T.; Marimuthu, A.; Hegde, M. S.; Ravishankar, N.; Madras, G. *J. Phys. Chem. C* **2007**, *111*, 830−839.
(6) Datye, A.; Bravo, J.; Nelson, T.; Atanasova, P.; Lyubovsky, M.; Pfefferle, L. *Appl. Catal., A* **2000**, *198*, 179−196.
(7) Singh, U.; Li, J.; Bennett, J.; Rappe, A.; Seshadri, R.; Scott, S. *J. Catal.* **2007**, *249*, 349−358.
(8) Li, J.; Singh, U. G.; Bennett, J. W.; Page, K.; Weaver, J. C.; Zhang, J.-P.; Proffen, T.; Rappe, A. M.; Scott, S.; Seshadri, R. *Chem. Mater.* **2007**, *19*, 1418−1426.
(9) Li, J.; Singh, U. G.; Schladt, T. D.; Stalick, J. K.; Scott, S. L.; Seshadri, R. *Chem. Mater.* **2008**, *20*, 6567−6576.
(10) Nishihata, Y.; Mizuki, J.; Akao, T.; Tanaka, H.; Uenishi, M.; Kimura, M.; Okamoto, T.; Hamada, N. *Nature* **2002**, *418*, 164−167.
(11) Ribeiro, F.; Chow, M. *J. Catal.* **1994**, *146*, 537−544.
(12) Escandon, L.; Ordonez, S.; Vega, A. *Chemosphere* **2005**, *58*, 9−17.
(13) Hicks, R.; Qi, H.; Young, M. *J. Catal.* **1990**, *122*, 280−294.
(14) Basile, A.; Paturzo, L. *Catal. Today* **2001**, *67*, 65−75.
(15) Cullis, C. F.; Nevell, T. G.; Trimm, D. L. *J. Chem. Soc., Faraday Trans. 1* **1972**, *68*, 1406.
(16) Muller, C.; Maciejewski, M.; Koeppel, R.; Baiker, A. *J. Catal.* **1997**, *166*, 36−43.
(17) Muller, C.; Maciejewski, M.; Koeppel, R.; Baiker, A. *Catal. Today* **1999**, *47*, 245−252.
(18) Ciuparu, D.; Altman, E.; Pfefferle, L. *J. Catal.* **2001**, *203*, 64−74.
(19) Groppi, G.; Cristiani, C.; Lietti, L.; Ramella, C.; Valentini, M.; Forzatti, P. *Catal. Today* **1999**, *50*, 399−412.
(20) Carstens, J.; Su, S.; Bell, A. *J. Catal.* **1998**, *176*, 136−142.
(21) Strobel, R.; Grunwaldt, J.; Camenzind, A.; Pratsinis, S.; Baiker, A. *Catal. Lett.* **2005**, *104*, 9−16.
(22) Grunwaldt, J.-D.; Maciejewski, M.; Baiker, A. *Phys. Chem. Chem. Phys.* **2003**, *5*, 1481−1488.
(23) Persson, K.; Ersson, A.; Jansson, K.; Iverlund, N.; Jaras, S. *J. Catal.* **2005**, *231*, 139−150.
(24) Roy, S.; Hegde, M. S.; Ravishankar, N.; Madras, G. *J. Phys. Chem. C* **2007**, *111*, 8153−8160.
(25) Roy, S.; Marimuthu, A.; Hegde, M. S.; Madras, G. *Appl. Catal., B* **2007**, *73*, 300−310.
(26) Bera, P. *J. Catal.* **2000**, *196*, 293−301.
(27) Baidya, T.; Dutta, G.; Hegde, M. S.; Waghmare, U. V. *Dalton Trans.* **2008**, 455.
(28) Roy, S.; Hegde, M. S.; Madras, G. *Appl. Energy* **2009**, *86*, 2283−2297.
(29) Singh, P.; Hegde, M. S. *J. Solid State Chem.* **2008**, *181*, 3248−3256.
(30) Gupta, A.; Waghmare, U. V.; Hegde, M. S. *Chem. Mater.* **2010**, *22*, 5184−5198.
(31) Baidya, T.; Gayen, A.; Hegde, M. S.; Ravishankar, N.; Dupont, L. *J. Phys. Chem. B* **2006**, *110*, 5262−5272.
(32) Baidya, T.; Gupta, A.; Deshpandey, P. A.; Madras, G.; Hegde, M. S. *J. Phys. Chem. C* **2009**, *113*, 4059−4068.
(33) Scanlon, D. O.; Morgan, B. J.; Watson, G. W. *Phys. Chem. Chem. Phys.* **2011**, *13*, 4279.
(34) Haneda, M.; Mizushima, T.; Kakuta, N. *J. Phys. Chem. B* **1998**, *102*, 6579−6587.
(35) Ciuparu, D.; Bozon-Verduraz, F.; Pfefferle, L. *J. Phys. Chem. B* **2002**, *106*, 3434−3442.
(36) Fu, Q. *Science* **2003**, *301*, 935−938.
(37) Gorte, R.; Zhao, S. *Catal. Today* **2005**, *104*, 18−24.
(38) Sharma, S.; Deshpande, P. A.; Hegde, M. S.; Madras, G. *Ind. Eng. Chem. Res.* **2009**, *48*, 6535−6543.
(39) Kao, L. C.; Hutson, A. C.; Sen, A. *J. Am. Chem. Soc.* **1991**, *113*, 700−701.
(40) Lunsford, J. *Catal. Today* **2000**, *63*, 165−174.
(41) Bradford, M.; Vannice, M. *Catal. Rev.* **1999**, *41*, 1−42.
(42) Tang, W.; Hu, Z.; Wang, M.; Stucky, G. D.; Metiu, H.; McFarland, E. W. *J. Catal.* **2011**, *273*, 125−137.
(43) Skrabalak, S. E.; Suslick, K. S. *J. Am. Chem. Soc.* **2006**, *128*, 12642−12643.
(44) Bérar, J.; Baldinozzi, G. Procedures for the refinement of incommensurate structures using XND. Coding issues for the refinement of incommensurate structures In *Newsletter No. 5, Commission on Crystallographic Computing*; Billinge, S., Chapuis, G., Cranswick, L.. Lifshitz, R., Eds.; International Union of Crystallography, 2005; pp 5−9.
(45) Palosz, B.; Grzanka, E.; Gierlotka, S.; Stel makh, S.; Pielaszek, R.; Bismayer, U.; Neuefeind, J.; Weber, H. P.; Proffen, T.; Dreele, Von, R.; Palosz, W. *Z. Kristallogr.* **2002**, *217*, 497−509.
(46) Palosz, B.; Grzanka, E.; Gierlotka, S.; Stel'makh, S.; Pielaszek, R.; Lojkowski, W.; Bismayer, U.; Neuefeind, J.; Weber, H. P.; Palosz, W. *GPHT* **2003**, *76*, 171−185.
(47) Palosz, B.; Grzanka, E.; Gierlotka, S.; Stelmakh, S. *Z. Kristallogr.* **2010**, *225*, 588−598.
(48) Williamson, G.; Hall, W. *Acta Metall.* **1953**, *1*, 22−31.
(49) Baidya, T.; Priolkar, K. R.; Sarode, P. R.; Hegde, M. S.; Asakura, K.; Tateno, G.; Koike, Y. *J. Chem. Phys.* **2008**, *128*, 124711.
(50) Priolkar, K. R.; Bera, P.; Sarode, P. R.; Hegde, M. S.; Emura, S.; Kumashiro, R.; Lalla, N. P. *Chem. Mater.* **2002**, *14*, 2120−2128.
(51) Brun, M.; Berthet, A.; Bertolini, J. *J. Electron Spectrosc.* **1999**, *104*, 55−60.
(52) Singh, P.; Hegde, M. S. *Cryst. Growth Des.* **2010**, *10*, 2995−3004.
(53) McGown, W. T.; Kemball, C.; Whan, D. A.; Scurrell, M. S. *J. Chem. Soc., Faraday Trans. 1:* **1977**, *73*, 632−647.